Tribology International 199 (2024) 109938

Contents lists available at ScienceDirect

Tribology International

journal homepage: www.elsevier.com/locate/triboint

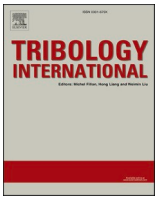

Influence of ZDDP tribofilm on micropitting formation and progression

Zaihao Tian [a,*], Ping Lu [b,a], Shuncai Wang [a], Daniel Merk [c], Robert Wood [a]

[a] National Centre for Advanced Tribology at Southampton, University of Southampton, Southampton SO17 1BJ, United Kingdom
[b] Centre for Manufacturing and Materials, Coventry University, Coventry CV1 5FB, United Kingdom
[c] Schaeffler Technologies GmbH & Co. KG, Schweinfurt 97421, Germany

ARTICLE INFO

Keywords:
Micropitting
ZDDP
Tribofilm
Friction

ABSTRACT

This paper presents insights into how Zinc Dialkyl Dithiophosphate (ZDDP) influences the formation and progression of micropitting. Experimental investigations were conducted using a twin-disc tribometer in rolling-sliding contacts under mixed or boundary lubrication conditions, focusing on the impact of ZDDP on micropitting in bearing steel samples. Results show that ZDDP reduces wear and increases surface friction by forming a tribofilm. This facilitates micropitting formation, but also retards the progression of micropitting. It highlights that understanding the chemical and mechanical interactions at the tribological interface is essential for designing effective mitigation strategies for managing micropitting and avoiding related issues in bearing applications.

1. Introduction

Micropitting is a type of fatigue failure that serves as a significant precursor to failures in machine elements such as in rolling element bearings and gears. These elements often employ heavily-loaded, rolling-sliding, and lubricated contacts [1,2]. Micropitting results from rolling contact fatigue (RCF) that arises from surface asperities undergoing repeated over-rolling and cyclic contact stresses. This phenomenon is especially prevalent in contacts operating under a low lambda ratio, signifying boundary and mixed lubrication regimes where the oil film thickness is not adequate to avert asperity contacts. With the continuous demand for higher power densities of mechanical systems, increased fuel efficiencies and thus lower energy losses, there is a corresponding shift towards lubricants with lower viscosities and smaller lambda ratios and thus higher potential for surface-to-surface interactions. As a consequence, these increased metal-to-metal interactions at the roughness asperity level have intensified, leading to a heightened occurrence of micropitting [3].

Micropitting appears as surface-initiated pits with depth of up to 20 μm [4,5]. It is not necessarily the primary failure mode, but it can lead to macropitting and accelerate the appearance of other failure modes like debris indentations, surface-initiated spalling, increased vibration, and in severe cases seizure [6–8]. Macropitting refers to the fully developed macroscopic pits with widths in the hundreds of micrometres and depths over tens of micrometres. These pits exhibit distinctive, discrete bottoms that intersect the surface at either steep or shallow angles. Macropitting can originate from surface defects, such as dents or micropits [8]. The transition from micropitting to macropitting is a complex process encompassing stages of plastic deformation and micro-cracking [9]. Within these stages, lubricant additives, particularly the anti-wear additive Zinc Dialkyl Dithiophosphate (ZDDP), emerge as significant influencers.

ZDDP is the most commonly used sulphur-phosphorus (S-P) based anti-wear additive. Predominantly in boundary or mixed lubrication regimes, ZDDP forms tribofilm during rubbing to reduce wear and protect the surface. ZDDP tribofilm typically exhibits a rough and irregular film with a thickness of approximately 50–150 nm thick [10,11]. The structure of ZDDP tribofilm is characterised by a foundational layer of iron/zinc sulfide, an intermediate layer enriched with iron/zinc phosphates and polyphosphate, and a surface layer composed of mixed oxide and zinc sulfide [12–14].

The role and implications of ZDDP tribofilm, especially its influence on micropitting, have been a focal point of research since the early 2000′s. Olver and his team, utilising a three-disc tribometer, discovered an inverse correlation between micropitting and mild wear. Their findings underscored the effect of ZDDP in reducing wear and increasing the possibility of micropitting production [15,16]. Subsequent studies by Spikes and his team further expanded on the tribofilm's role in influencing friction and its impact on micropitting. Tests were conducted by a ball-on-disc Mini-Traction Machine (MTM) to develop

* Corresponding author.
E-mail address: Zaihao.Tian@soton.ac.uk (Z. Tian).

https://doi.org/10.1016/j.triboint.2024.109938
Received 25 September 2023; Received in revised form 12 April 2024; Accepted 30 June 2024
Available online 8 July 2024

deeper understanding on the dynamics between ZDDP tribofilm growth rate and micropitting evolution. Their findings revealed that although the role of ZDDP in reducing surface wear was commendable, it enhanced micropitting risks by inhibiting the proper running-in of component surfaces [10]. Additional studies measured ZDDP tribofilm thickness, friction forces induced by the tribofilm, and their cumulative effects on micropitting, emphasising the multifaceted nature of these interactions [11,17,18]. These studies demonstrated that ZDDP tribofilm can elevate friction between contact surfaces. Detailed mechanisms of ZDDP tribofilm's frictional behaviour was studied recently by Sato and his colleagues. They demonstrated that the robust adhesive force of the ZDDP tribofilm significantly contributes to the rise in friction levels [19]. Brizmer from SKF conducted experimental and theoretical studies on tribofilm formation and highlighted that while the tribofilm was advantageous for surface protection from wear, it could heighten micropitting vulnerability due to higher friction levels. This increase in friction induced elevated localised shear stress, thereby accentuating the risk of micropitting [20].

However, other research provides opposite perspectives on the issue. A 2019 study from Lulea showed that micro-pitting damage is a function of surface roughness combination and hardness difference among other factors. Their study found that ZDDP additive in engine oil protected rougher surfaces, promoting wear on smoother surfaces, effectively eliminating the micro-pitting damage mode [21]. Airey and colleagues from Rolls-Royce conducted tests with base oil and ZDDP-enriched oil separately and found that ZDDP led to faster progression and larger amount of micropitting but the dimension of micropitting was smaller. In contrast, the base oil exhibited slower initiation of micropitting, but the micropits quickly propagated into severe macropitting [22]. The underlying physics responsible for this slowed progression of micropitting in the ZDDP test, however, remains not fully elucidated.

The relationship between friction and micropitting has also been studied widely. As early as 2003, Benuzzi employed a Finite Element Method (FEM) model to assess the stress intensity factor range and track crack progression under rolling-sliding contact conditions. This study unveiled that stress intensity factors are influenced by friction force on both contact surfaces and crack faces [23]. It was found crack progression could be accelerated by high contact surface friction while retarded by high crack face friction. Similar conclusions was drawn by M.C. Baietto and co-authors [24]. Parametric studies on the influence of the friction coefficient between the crack faces have been conducted. Higher friction coefficients were found to reduce the value of the stress intensity factor in mode II and therefore slow the crack growth.

As discussed above, while extensive research has been conducted on the role of ZDDP additive in micropitting, conflicting perspectives persist regarding its exact influence. Moreover, there remains a gap in understanding the interplay of crack chemistry, friction, and micropitting behaviour. To address these research challenges, the aim of this paper is to provide further insight into the impact of ZDDP on the formation and progression of micropitting. This is achieved by conducting tribological experiments on a twin-disc tribometer with particular focus on the mechanisms of ZDDP's role in wear protection and friction. The influence of ZDDP is isolated and studied under different lambda ratios and sliding conditions. Surface topography of samples and friction are analysed to reveal the mechanisms through which ZDDP tribofilm influences micropitting. These findings are not only crucial for understanding the underlying physics governing micropitting performance but also for optimising non-pitting oil formulations for bearing applications.

2. Test methodology

2.1. Experimental equipment

Experiments for this study were carried out using a Phoenix Tribology TE74 twin-disc tribometer, which is illustrated in Fig. 1. The

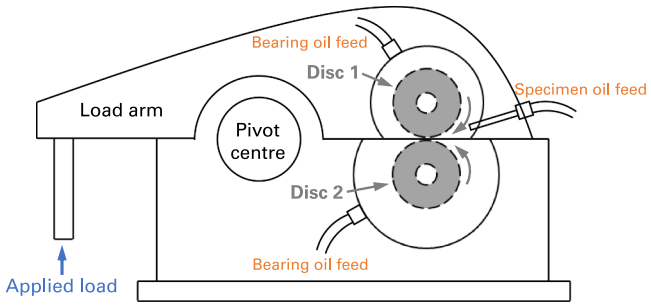

Fig. 1. An illustration of the TE74 twin-disc tribometer.

TE74 tribometer is designed to study wear and RCF under lubricated rolling and rolling-sliding conditions. The test rig incorporates a pair of discs mounted on parallel shafts which can be driven independently by three-phase motors. In this configuration, controlled sliding can be induced into the disc contact by adjusting the rotating speeds of the discs, which can range from 200 to 2000 rpm. The machine can apply up to 12 kN onto the contact by employing a servo controlled pneumatic actuator equipped with force transducer feedback. The actuator applies load onto the contact through the movement of a pivot positioned on the load arm. The drive to the lower disc incorporates an in-line torque transducer, facilitating the measurement of the system's input torque with a sampling rate of 10 Hz. The coefficient of friction can be calculated by: input torque/(radius of lower disc × applied load). The lubricant is pumped directly to the disc contact and support bearings by a recirculation line incorporating a 40 μm filter downstream of the test cell. Additionally, a heating element installed in the oil tank serves to heat oil from ambient conditions to a pre-set temperature of up to 180°C.

Before and after tests, the discs were ultrasonically cleaned with acetone for 10 minutes and dried using high-pressure air. The roughness of discs was measured using a contact-based profilometer, Intra Touch (Taylor Hobson, Leicester, UK). This device performs a single 2D profile, and calculates surface parameters such as form, waviness and roughness. A stylus vertical range of 1 mm with a vertical resolution of 4 nm was employed for the high precision roughness measurement. The surface topography of discs was measured using a high-resolution non-contact optical 3D surface measurement device, Alicona G4 InfiniteFocus profilometer (Alicona Imaging GmbH, Raaba, Austria). The system integrates features of an optical profiler and a micro coordinate measurement device. Such integration facilitates comprehensive surface characterisation in a single measurement with a vertical resolution of up to 10 nm.

To quantify the extent of pitting, measurements were performed on the area fraction, width, and depth of pits. To estimate the area fraction and width, optical images obtained by Alicona were converted into binary formats using ImageJ software, where black pixels represented the presence of cracks or pits and white pixels represented their absence. An example of the process is shown in Fig. 2(a). The measurement of the fraction of the black area enabled a quantitative representation of the extent of pitting. For measuring the depth of the pits, the pitted areas were observed using the 3D imaging capability of Alicona, which enables the measurement of various surface irregularities. By analysing the depth information in the acquired images, the system provided quantitative data on the depth of pits. Subsequently, corresponding colour maps were generated to visually represent the pits as shown in Fig. 2(b). To ensure a comprehensive assessment, four randomly selected areas on each disc were chosen for the measurements.

A JEOL JSM-7200 F scanning electron microscope (SEM) equipped with EDAX EDS (Energy Dispersive X-Ray Spectroscopy) detector, manufactured by JEOL Ltd., Tokyo, Japan, was used to observe cracks and pits at higher magnifications and detect the presence of ZDDP tribofilm. The main features of the SEM are "In-Lens SchottkyPlus" technology-based electron optics, Gentle Beam (GB) mode, Through-

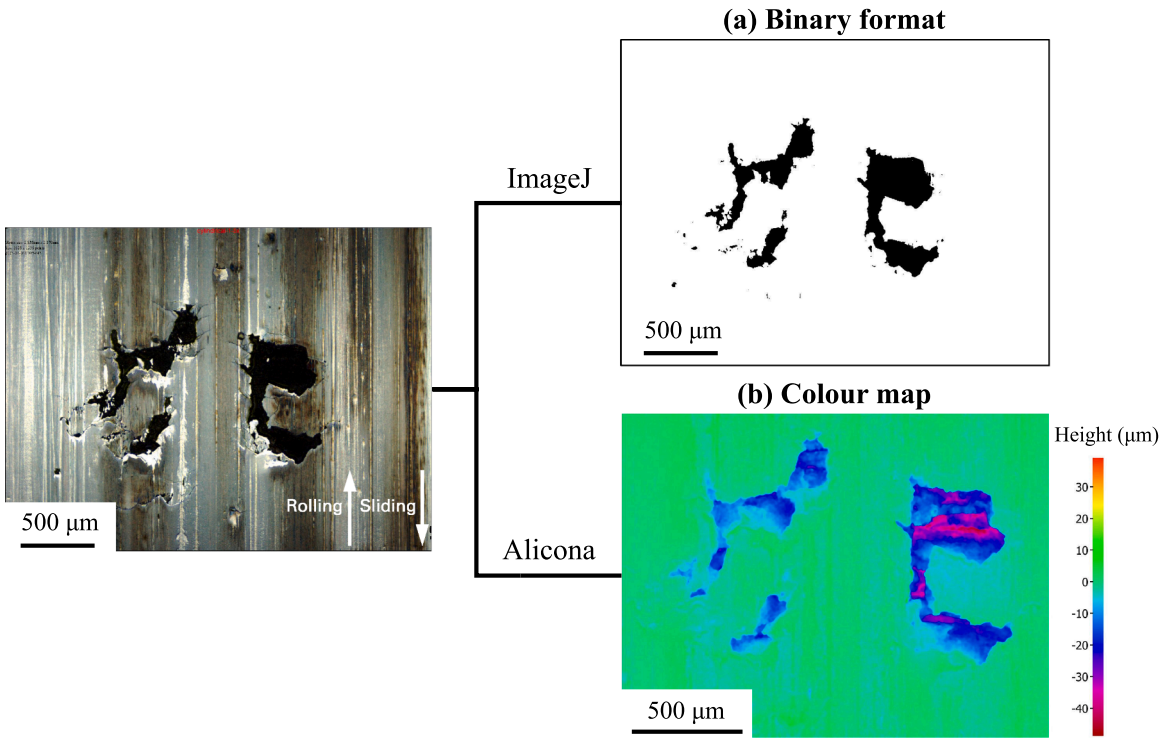

Fig. 2. Binary format converted from an original image using ImageJ, and colour map generated using Alicona.

The-Lens System (TTLS) that enables high resolution observation at low accelerating voltage and control the number of low-energy signals to be detected by the upper detectors, and a hybrid objective lens that combines magnetic-lens and electrostatic-lens.

2.2. Materials

In the twin-disc setup in the TE74 tribometer, a pair of discs made of AISI 52100 bearing steel were used for generating pitting. The 39 mm diameter disc, termed "smooth disc", exhibited a roughness parameter, R_q (Root Mean Square) of 0.03 μm and adopted a cylindrical surface geometry. The 41 mm diameter discs, referred as "rough disc", had a higher roughness R_q of 0.26 μm and featured a crowned surface geometry with a transverse diameter of 100 mm. Both types of discs had a width of 12 mm, as illustrated in Fig. 3. The design simulated the contact between rollers and raceways in rolling element bearings and ensured a self-aligning elliptical contact, which effectively minimised stresses induced by edges. Furthermore, this configuration ensured that wear tracks were positioned centrally, facilitating effective observations of surface damage that generated during testing.

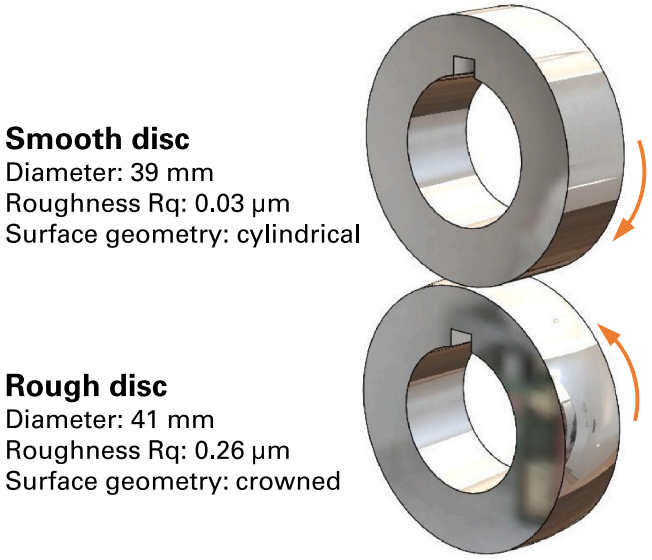

Fig. 3. Schematic drawing of the discs used in TE74 twin-disc tribometer.

To investigate the influence of ZDDP additive on micropitting formation and progression, base oil only and base oil + ZDDP tests were conducted. The base oil used was PAO oil "Durasyn 168 poly-alphaolefins" provided by INEOS Oligomers Group. PAO oil is a type of hydrogenated synthetic hydrocarbon base fluid for use in fully and partially synthetic, premium, long-drain lubricating oils, hydraulic fluids, or transmission fluids. Due to its limited wear properties, it has also been widely used in bearing steel tests to study the mechanisms of micropitting [6,15,21]. Details of Durasyn 168 are shown in Table 1. The ZDDP additive used was HiTEC 1656 primary-secondary mixed ZDDP containing 8.35 % zinc, 9.2 % phosphorus, and 17.8 % sulphur, provided by Afton Chemical Corporation. In base oil + ZDDP tests, Durasyn 168 base oil was blended with 2 wt% ZDDP. The ZDDP-enriched oil was prepared by slowly adding the ZDDP into Durasyn 168 while stirring using a magnetic stirrer to blend the mixture and ensure a homogeneous mixture.

2.3. Test conditions

Before the commencement of pitting tests, baseline tests operating under mixed and elasto-hydrodynamic lubrication conditions were conducted to ensure accurate measurement of friction in a controlled

Table 1
Properties of Durasyn 168 base oil.

Kinematic viscosity, cSt, 100 ℃	Kinematic viscosity, cSt, 40 ℃	Viscosity index	Flash point, ℃	Specific gravity (15.6/15.6 ℃)
7.8	47.5	136	> 245	0.831

environment. Subsequently, eight pitting tests were conducted on the TE74 tribometer, with the test conditions outlined in Table 2. These conditions were established based on two- or three-disc experiments in previous studies [1,6,15,21,25,26] in which micropitting was successfully produced. In these experiments, the maximum contact pressure was controlled between 1.7 to 4.7 GPa, and the lambda ratio was varied between 0.1 to 0.7 to obtain boundary lubrication conditions conducive to induce micropitting. The oil temperature was maintained between 65 to 100 ℃ to promote the formation of ZDDP tribofilm. Slide-to-roll ratios (SRR) ranging from 1 % to 30 % were employed to ensure appropriate sliding conditions for fatigue crack initiation and ZDDP tribofilm formation. It was widely observed in rolling-sliding contacts, the discs operating at slower speeds exhibited a higher incidence of micropitting formation. The durations of the experiments were typically set between 4 to 9 million cycles to ensure an adequate number of stress cycles for micropitting occurrence.

Referencing the use of maximum contact pressures ranging from 1.7 to 4.7 GPa in tribometer tests [1,6,15,21,25] and 2.17 GPa in bearing tests [26], a maximum contact pressure of 2.5 GPa was applied in all the tests in this work. In Tests 1, 2, 3 and 4, the lambda ratio was set as 0.23 to achieve boundary lubrication conditions, and the SRR was set as − 10 % to simulate the contact conditions between rollers and raceways in rolling element bearings where micropitting is commonly observed [26]. A negative SRR means smooth discs were slower than rough discs. Tests 1 and 2 were conducted for 1.5 million cycles to specifically observe the initiation of surface cracks and micropitting. Conversely, Tests 3 and 4 were extended to 6 million cycles to monitor the progression of micropitting. Furthermore, Tests 5 and 6 aimed to investigate the influence of ZDDP under different lambda ratios with a higher lambda ratio of 0.74. Tests 7 and 8 explored the effect of ZDDP under different SRRs, employing a larger SRR of − 20 %.

3. Results and discussion

3.1. Imaging micropitting and macropitting

Following the completion of the TE74 tests, the discs were observed using optical and electron microscopy techniques to analyse the failure modes and mechanisms. Initial inspections were performed using the Alicona microscope system and the outcomes are presented in Fig. 4. Cracks and pits were uniformly distributed across the wear tracks on smooth discs. To illustrate the topography and extent of pitting, three images at random locations of each smooth disc are presented in Fig. 4. The width, depth, and fraction of pits, measured using the methods presented in Fig. 2, are illustrated in Fig. 5. In this work, micropits and macropits are distinguished according to depth. Pits with a depth of less than 20 μm are classified as micropits [4,5], while pits with a depth exceeding tens of microns are categorised as macropits [8], as illustrated in Fig. 5(b). The width of the pits is not considered a criterion, as the joined pits could potentially impact the differentiation.

In the base oil only test, with a lambda ratio of 0.23, small and shallow cracks initiated on the smooth disc around or slightly prior to 1.5 million cycles (Test 1). Subsequently, by 6 million cycles (Test 3), the cracks had developed into pits characterised as macropits, with widths measuring in the hundreds of microns and depths of tens of microns. This resulted in a significant increase in damaged area. In contrast, with the use of ZDDP-enriched oil, pits with depth up to 20 μm had formed at 1.5 million cycles (Test 2), characterised as micropits. However, after 6 million cycles (Test 4), their dimensions and areas experienced minimal growth.

In the test conducted under a higher lambda ratio of 0.74 using the base oil (Test 5), neither cracks nor pits were observed by 6 million cycles. However, in contrast, in the base oil + ZDDP test (Test 6), micropits were evident on the smooth disc. Under a higher SRR of − 20 %, macropits were observed on the smooth disc after 6 million cycles in the base oil only test (Test 7). Conversely, in the base oil + ZDDP test (Test 8), smaller micropits were observed on the smooth disc. The observations indicate that the use of ZDDP resulted in the earlier formation of micropits (Test 2 and 6); however, the rate of micropit evolution was slower (Test 4 and 6). Referring to [7,21,22], the fraction of pitting areas is employed to evaluate the extent of pitting. It is revealed from Fig. 5(c) that for both base oil and base oil + ZDDP tests, a higher lambda ratio of 0.74 resulted in minimal pitting damage. When using base oil only, an increased SRR of − 20 % resulted in less pitting (Test 7).

As outlined in Table 2, Test 1 (1.5 million cycles) and 3 (6 million cycles) had the same test conditions except for duration, and Test 2 (1.5 million cycles) and 4 (6 million cycles) likewise had the same test conditions with differing durations. The discs used in Test 3 and 4 were not removed from the TE74 tribometer for interval observations at 1.5 million cycles, as this required disassembly and reassembly, potentially influencing the positioning of the contact patch and consequently impacting generation of pits and the measurement of the coefficient of friction.

To explore the repeatability of Test 1 and 3, as well as Test 2 and 4, vibration signals obtained during these tests were analysed and compared. The vibration monitoring and signal processing methods were detailed in [27]. The root mean square (RMS) values of the vibration signals acquired from the four tests are presented in Fig. 6. Slight differences were observed between the vibration RMS values of Tests 1 and 3, as well as Tests 2 and 4, within the initial 1 million cycles, which could potentially be attributed to variations during the running-in process. However, by 1.5 million cycles, the signals for Tests 1 and 3 converged to comparable levels. Similarly, the signals for Tests 2 and 4 also converged by 1.5 million cycles. As explained in [27], the source of vibration was attributed to cracks and pits on smooth discs and the vibration RMS represented the extent of damage. The comparable level of vibration RMS at 1.5 million cycles indicated similar extent of damage was produced, therefore indicating the repeatability of Tests 1 and 3, and Tests 2 and 4.

3.2. Formation mechanisms of micropitting and macropitting

Fig. 4 indicates that pitting damage was exclusively observed on the smooth discs in smooth-rough combinations. The phenomenon aligns with findings from previous studies [7,21]. These studies have demonstrated that a smooth-rough contact configuration promotes the development of surface-initiated cracks and pits on the smooth surfaces. The

Table 2
Test conditions for the base oil and base oil + ZDDP tests.

No.	Oil	Max. contact pressure (GPa)	Entrainment speed (m/s)	Lambda ratio	Oil temp (℃)	Slide-roll ratio (%)	Duration (million cycles)
1	Durasyn 168	2.5	1.29	0.23	100	-10	1.5
2	Durasyn 168 +ZDDP	2.5	1.29	0.23	100	-10	1.5
3	Durasyn 168	2.5	1.29	0.23	100	-10	6
4	Durasyn 168 +ZDDP	2.5	1.29	0.23	100	-10	6
5	Durasyn 168	2.5	2.58	0.74	60	-10	6
6	Durasyn 168 +ZDDP	2.5	2.58	0.74	60	-10	6
7	Durasyn 168	2.5	1.36	0.24	100	-20	6
8	Durasyn 168 +ZDDP	2.5	1.36	0.24	100	-20	6

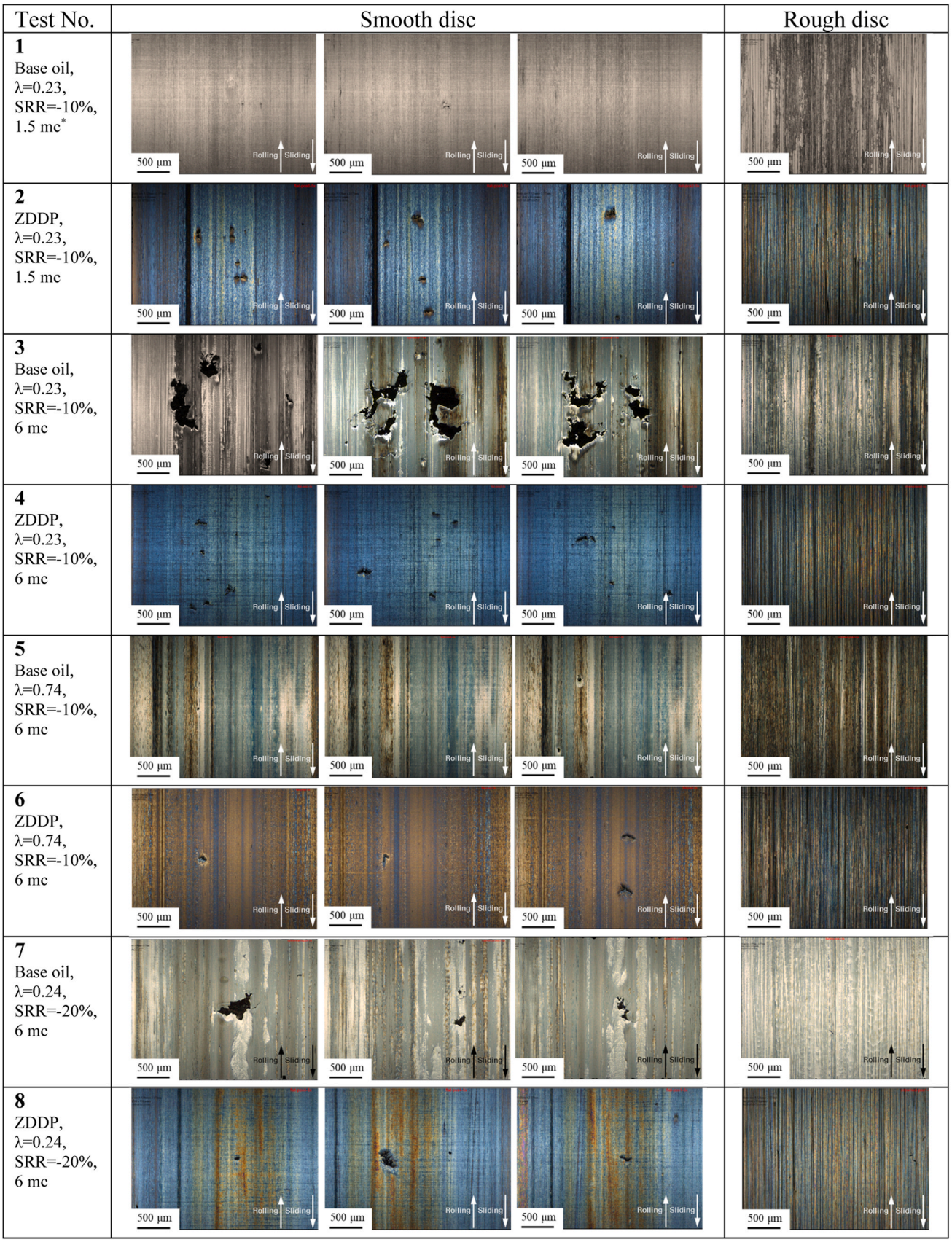

Fig. 4. Post-test surface topography images of discs for Tests 1–8.

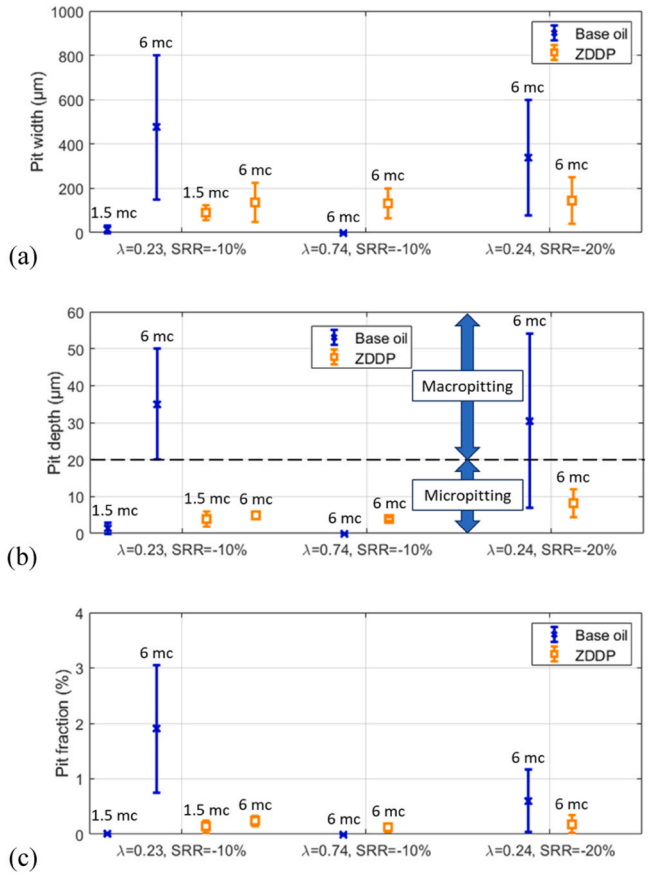

Fig. 5. (a) Pit width, (b) depth, and (c) fraction for Tests 1–8.

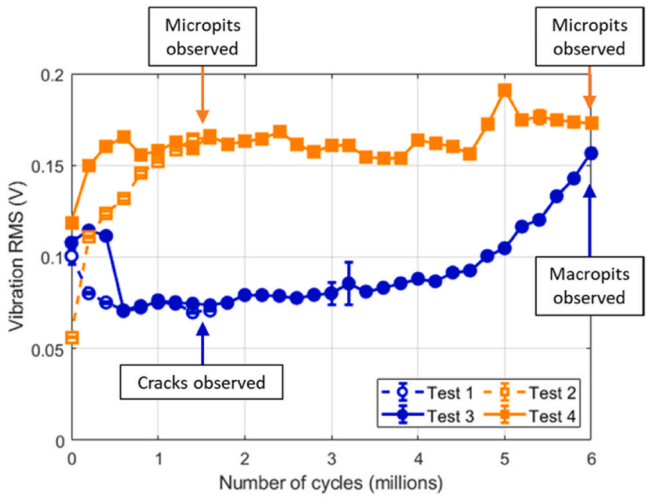

Fig. 6. RMS values of vibration signals collected from Tests 1–4. Signal acquisition and processing methods see [27].

likely explanation for this is the stress history from the fatigue micro-cycles imposed by surface roughness [21,28]. In boundary or mixed lubrication conditions where asperity contacts are severe, the stress history is imposed by the dominant rougher surface upon the smoother one. When a rough surface moves against the smooth one, the smooth surface experiences a fluctuation in pressure from the rough surface. Moreover, the individual asperities on the surface create localised contacts, leading to a reduction in the actual contact area. This, in turn, generates higher local stresses close to the surface, thereby initiating the onset of cracks and pitting on the surface [28].

To study the mechanism behind the formation of macropitting and micropitting, a detailed analysis of the pitting morphology on both the surface and subsurface was conducted using the SEM. Fig. 7 shows representative examples of macropitting produced in Test 3 on surface and cross-section views. The plane of the section is parallel to the rolling-sliding direction and passes through the middle of the pit in transverse direction as shown in Fig. 7(a). On the surface the macropit was characterised by the separation of fine flakes or platelike structures comprising the embrittled metallic matrix. Extensive cracks were observed in the vicinity of the macropit. The cross-section view shown in Fig. 7(b) was obtained by cutting through the centre of the wear tracks along the rolling and sliding direction. It is evident that cracks originated from the surface at a shallow angle of approximately 13° and generally propagated against the sliding direction into the material. The cracks interacted with each other, resulting in the removal of a segment of surface material and generating macropits with a saw-tooth bottom appearance. The depth of macropits exceeded 20 μm and cracks tended to continue propagating into subsurface with the depth of approximately 118 μm, accompanied by additional cracks branching to produce secondary damage.

Fig. 8 shows a representative example of micropitting produced in Test 4 on the surface and cross section views. As shown in Fig. 8(a), the micropit had a width of around 200 μm and displayed a 'crescent moon' shape on the surface. On the cross-section view shown in Fig. 8(b), similar to the observation of macropitting, the crack propagated counter to the sliding direction into the material at a shallow angle of roughly 7° to the surface. Subsequently the interaction between cracks generated a micropit with a depth of approximately 5 μm. The maximum depth of the crack was only around 13 μm, and there was no distinct inclination for substantial further propagation.

It is notable that in both tests, the cracks exhibited a tendency to propagate in a direction opposing the direction of sliding which aligns with findings in [29,30]. To investigate the mechanism of crack propagation, the etched cross-section of the micropitted disc in Test 4 using a 2 % Nital solution was observed as shown in Fig. 9(a). It was seen that the martensite phase near the surface was shaped into inclined lines and the cracks followed the direction of the material flow. This phenomenon could be explained by the plastic deformation induced by sliding friction in the near-surface region as illustrated in Fig. 9(b). Within the near-surface region, the material experiences plastic deformation due to shear stress induced by sliding friction. The strain is pronounced closer to the surface, leading to material flow against the sliding direction. Initiated from the base of deformed asperities, cracks naturally tend to propagate along the direction of deformation.

3.3. Identification of ZDDP tribofilm on contact surfaces and its effect on micropitting formation

To identify the presence of ZDDP tribofilm and analyse its chemical composition, SEM/EDS analysis was performed on surfaces of the discs tested with the ZDDP-enriched oil. ZDDP tribofilm was identified on all the discs in these tests. As an illustration, Fig. 10 shows the SEM image of a micropitted area on the smooth disc in Test 2 ($\lambda = 0.23$, SRR=−10 %, 1.5 million cycles) and the corresponding EDS profile. The EDS profile confirmed the presence of peaks of zinc, phosphorus, and sulphur, which are characteristic elements derived from ZDDP. The weight proportion of these elements are listed in Table 3.

Fig. 11 illustrates the roughness parameter R_q of the discs, as measured in the axial direction (perpendicular to the rolling-sliding direction) by Intra Touch. The roughness measurements were conducted in regions without pits. After 6 million cycles in the base oil + ZDDP tests, R_q of the smooth discs increased by 33–80 %, and R_q of the rough discs increased by 3–12.5 %. The increase in R_q can be attributed to the formation of ZDDP tribofilm. ZDDP tribofilm protects surfaces from wear and maintains asperities [10,11,31]. Moreover, the tribofilm is

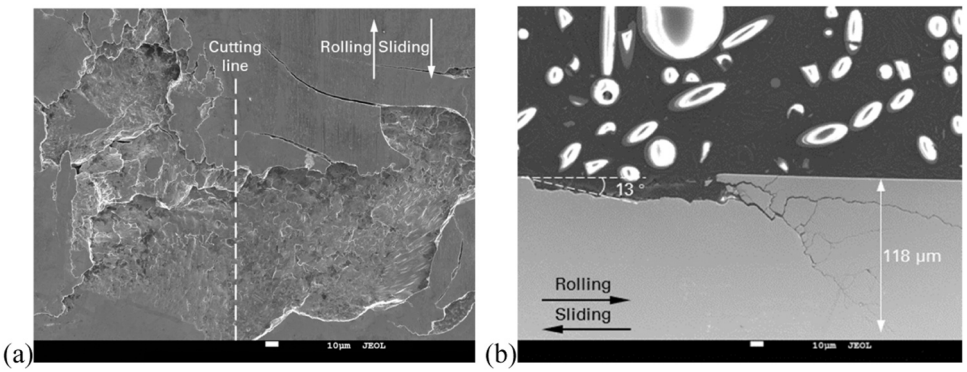

Fig. 7. SEM observations of macropitting on (a) surface and (b) cross section of the smooth disc in base oil only test (Test 3).

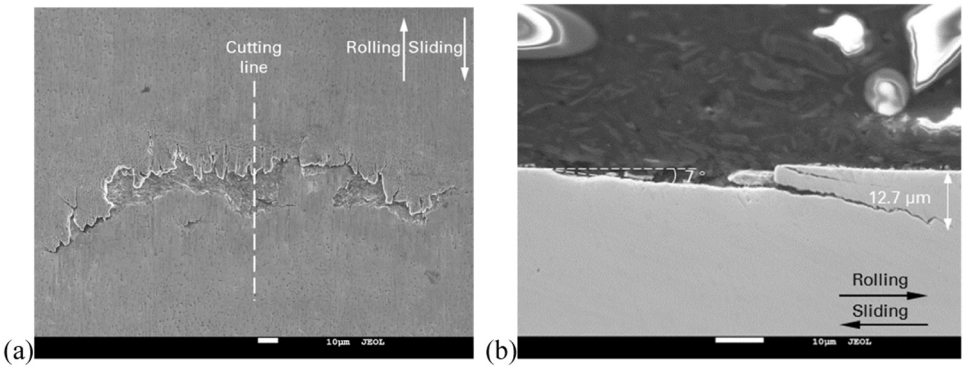

Fig. 8. SEM observations of micropitting on (a) surface and (b) cross section of the smooth disc in base oil + ZDDP test (Test 4).

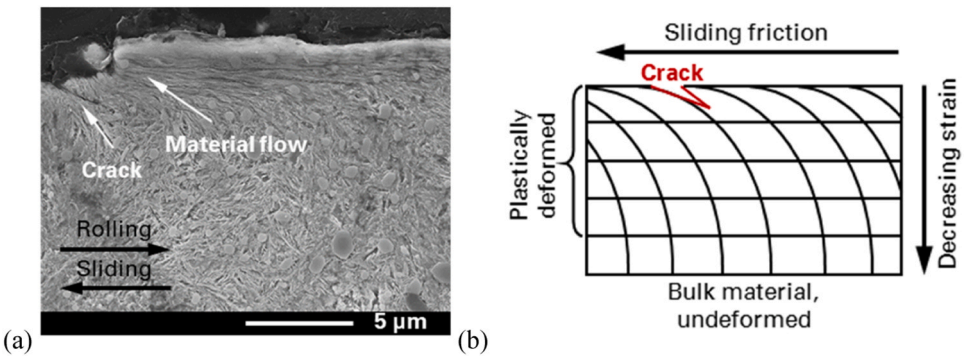

Fig. 9. (a) Observation of plastic deformation and crack propagation in Test 4; (b) Schematic of plastic deformation due to sliding friction.

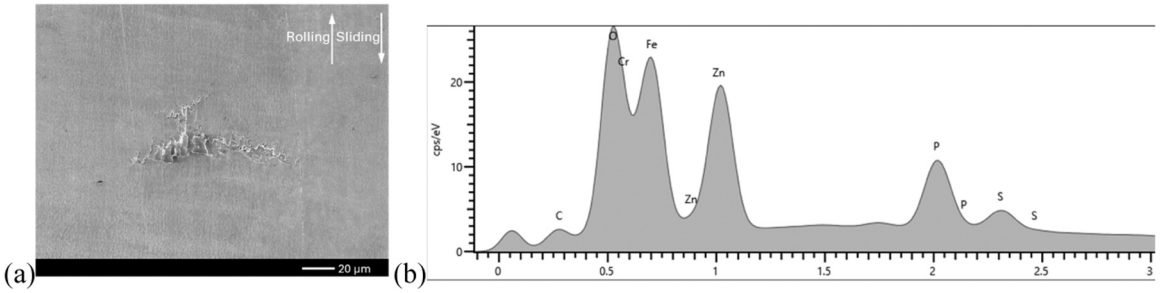

Fig. 10. (a) SEM image of the smooth disc in Test 2 and (b) corresponding EDS profile.

composed by rough micron-scale circular or elongated pads, reaching up to 150 nm in thickness [10,11]. The preservation of the original asperities and the thickness of ZDDP tribofilm contributed to the increased roughness.

In the base oil only tests, the disc surface roughness exhibited a pronounced increase when compared to the ZDDP tests, indicating

Table 3
ZDDP elements and weight % of ZDDP tribofilm.

Element	Fe	Cr	O	Zn	P	S
Weight %	57.76	1.46	12.82	19.46	6.11	2.38

higher wear rates. Without ZDDP tribofilm which controls wear by limiting direct contact of the two rubbing surfaces, the wear process was faster and more severe in direct metal-metal contacts lubricated solely by the base oil. As a result, wear induced the formation of irregularities and alterations in surface topography, leading to a notable increase in surface roughness.

The wear process in base oil only tests can be one reason for the delayed formation of pits (Tests 1 and 5) as observed in Fig. 4. Pitting is a material fatigue phenomenon caused by repeated rolling-sliding contacts. Fatigue cracks typically initiate at locations of stress concentration, such as surface asperities. These stress concentrations lead to localised increases in stress. When the stress exceeds a certain threshold, microscopic cracks can develop at the surface asperities. Under cyclic loading, these cracks may propagate, resulting in the formation of pits through material loss. Wear, on the other hand, is a mechanical process where material is removed from the surface. This action alters the surface topography and removes stress concentration points i.e. surface asperities. Furthermore, wear removes the uppermost fatigued layers, therefore reducing the accumulation of pitting damage [7,32,33].

Under a lambda ratio of 0.23, by 1.5 million cycles, the base oil only test (Test 1) exhibited a larger roughness compared to the base oil + ZDDP test (Test 2), as shown in Fig. 11 (a). This indicates formation of more wear. Consequently, more asperities were removed, making it more challenging for cracks to initiate and propagate. Therefore, the formation of pits was delayed. In contrast, in the base oil + ZDDP test (Test 2), ZDDP tribofilm retained asperities, facilitating sufficient stress cycles for the initiation and progression of cracks into micropits. Under a higher lambda ratio of 0.74, the base oil only test (Test 5) similarly exhibited a greater increase in roughness compared with the base oil + ZDDP test (Test 6) as shown in Fig. 11 (b). Additionally, a larger separation of contact surfaces led to fewer asperity contacts. Therefore, crack initiation was further delayed, and no cracks were observed until 6 million cycles.

Upon comparing Fig. 11 (a) and (c), it is observed that in the base oil tests, R_q of the smooth disc in Test 7 ($\lambda = 0.24$, SRR=−20 %) underwent a greater increase compared to Test 3 ($\lambda = 0.23$, SRR=−10 %). Despite the lambda ratio being comparable in these two tests, the larger increase in roughness in Test 7 was attributed to increased sliding. With the heightened sliding, a higher wear rate was resulted. Consequently, an increased SRR of − 20 % resulted in reduced fraction of pitting area as illustrated in Fig. 5(c).

Fig. 12 depicts the evolution of the coefficient of friction in Tests 1 to 8. It is observed that under the same test conditions except for lubricants, tests conducted with the ZDDP-enriched oil exhibited higher coefficients of friction compared to those conducted with the base oil. The increased friction can be attributed to the increased adhesion forces induced by ZDDP tribofilm. The correlation between the adhesion force and nano-friction force has been confirmed by previous research [19].

The earlier formation of micropitting in the base oil + ZDDP tests (Tests 2 and 6) can also be attributed to the higher surface friction induced by the ZDDP tribofilm. In the modelling study presented in [23], in a general rolling-sliding contact, the possibility and mode of crack propagation were studied by determining ranges of mode I (tensile) and mode II (shear) stress intensity factor (K), ΔK_I and ΔK_{II}. The stress intensity factor range can be calculated from the maximum and minimum stress intensity for a cycle, and the crack growth rate is found to increase

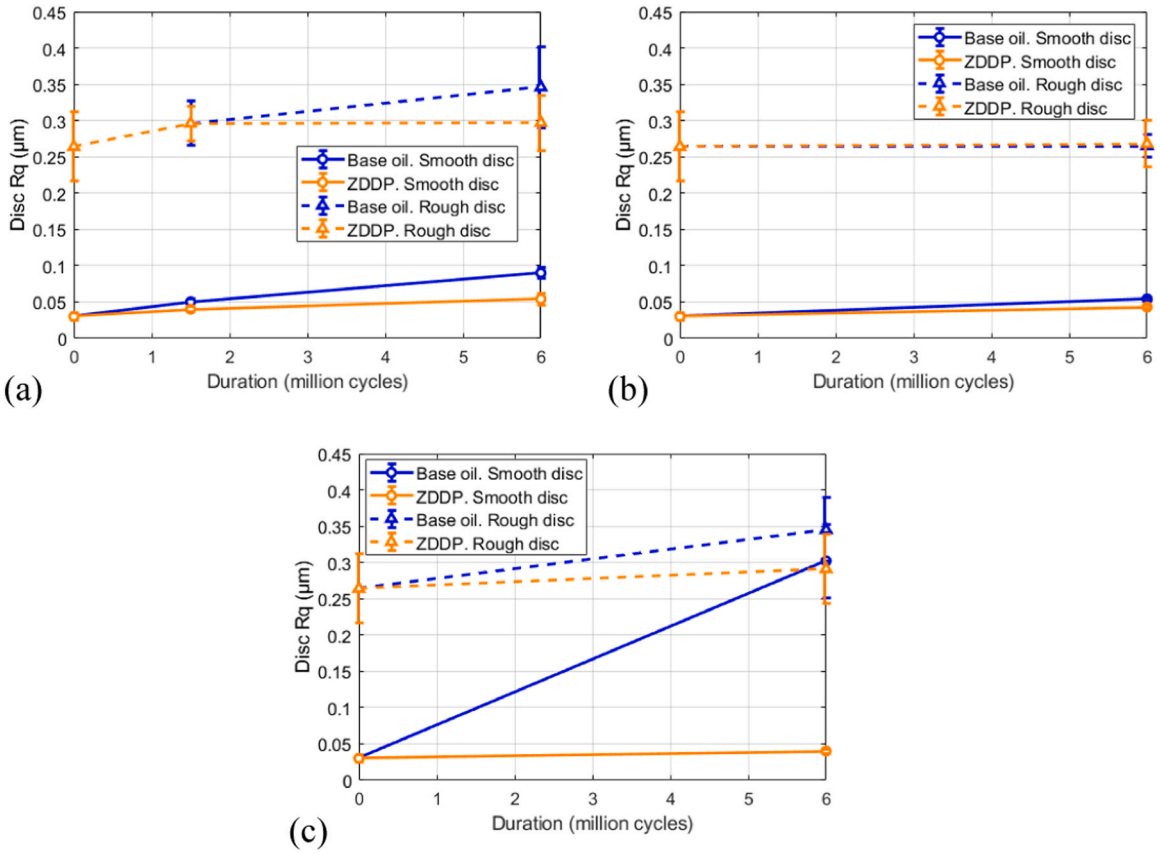

Fig. 11. Roughness parameter R_q of discs after tests with (a) $\lambda = 0.23$, SRR= −10 % (Tests 1 to 4), (b) $\lambda = 0.74$, SRR= −10 % (Tests 5 and 6), and (c) $\lambda = 0.24$, SRR= −20 % (Tests 7 and 8).

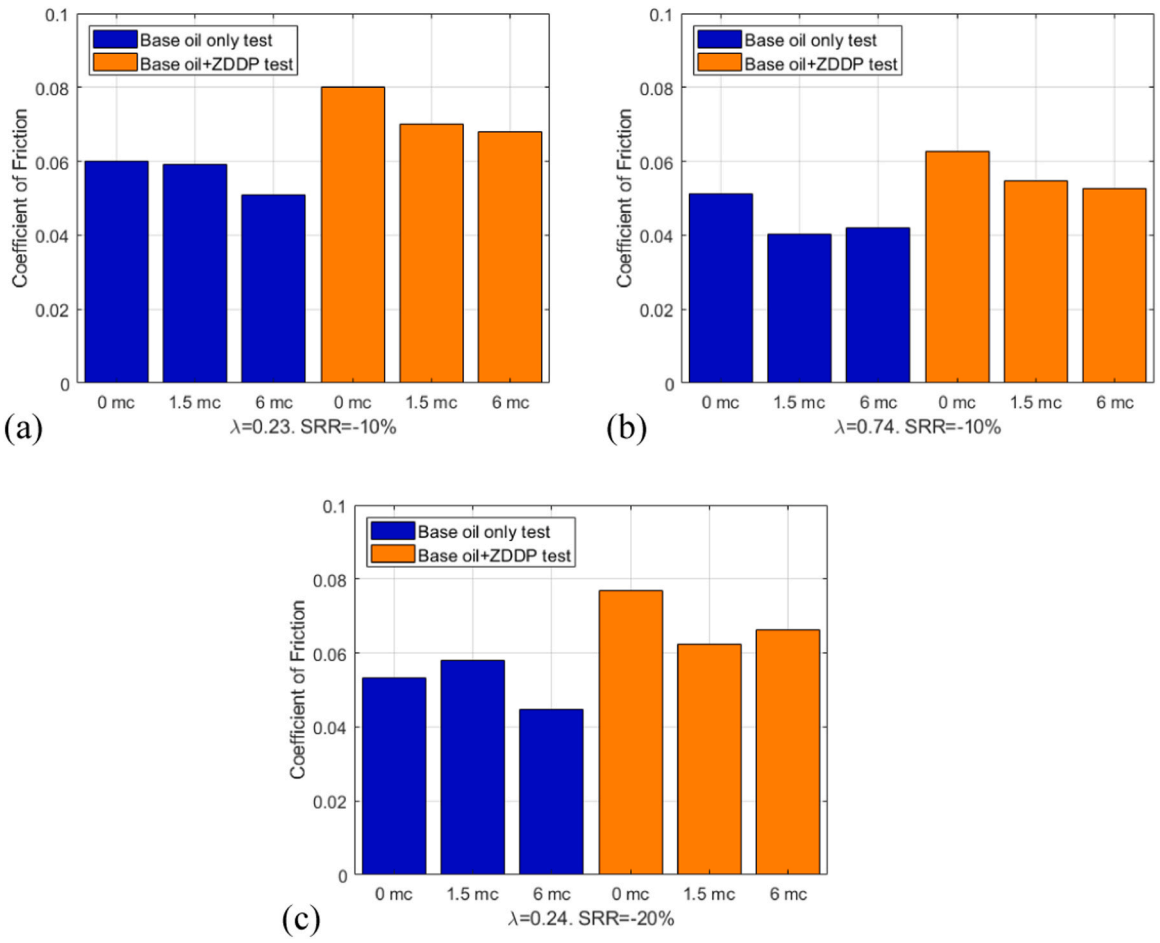

Fig. 12. Coefficient of friction for various numbers of cycles with (a) λ = 0.23, SRR= −10 % (Tests 3 and 4), (b) λ = 0.74, SRR= −10 % (Tests 5 and 6), and (c) λ = 0.24, SRR= −20 % (Tests 7 and 8).

with the increase in the range of stress intensity factor [18,23]. It was demonstrated that under a wide range of crack propagation angles, both ΔK_I and ΔK_{II} increase with the surface friction f_s [23]. As a result, tensile and shear stresses increase at the rear of the contact region [18], as indicated in Fig. 13. This potentially promotes crack initiation. Once cracks initiates, their interactions contribute to the formation of micropitting.

Under a higher lambda ratio of 0.74, the coefficient of friction was lower compared to lambda ratios of 0.23–0.24. This can be understood by considering the relationship between coefficient of friction and lubrication regime. At higher lambda ratios, the lubricant film thickness between the contacting surfaces is increased. This thicker lubricant film serves to separate the surfaces more effectively, reducing direct asperity contact and thus lowering friction. As indicated in Fig. 5(c), a higher lambda ratio of 0.74 resulted in minimal pitting damage, which could be due to the low friction.

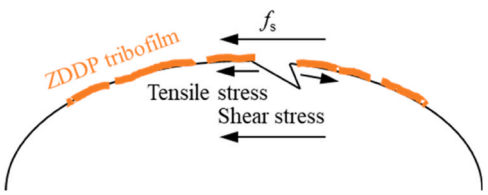

Fig. 13. Effect of surface friction on near surface stresses and crack initiation.

3.4. Identification of ZDDP tribofilm on crack faces and its effect on micropitting progression

To explore the presence of ZDDP tribofilm within the cracks in the base oil + ZDDP tests, SEM/EDS investigation was conducted on cross sections of cracks, and examples of the results are depicted in Fig. 14. In Fig. 14 (a), element distributions were obtained using EDS line analysis at the disc surface and two positions along a crack path in Test 4 (λ = 0.23, SRR=−10 %, 6 million cycles): the crack mouth and crack tip.

It is evident from Fig. 14 (b) that the ZDDP elements, including zinc, phosphorus, and sulphur, were concentrated on the disc surface. In Fig. 14 (c) the ZDDP elements were prominently concentrated on the crack faces at the crack mouth, while not detected inside the crack. In Fig. 14 (d), similarly high concentrations of ZDDP elements were observed at the crack tips. Due to the close proximity of the crack faces at the tip, the presence of ZDDP elements on the two crack faces could not be distinguished.

As discussed in Section 3.3, ZDDP tribofilm was identified on disc surfaces. Comparing Fig. 14 (c) and (d) with (b), the film on crack faces had the same elemental composition with that on the disc surface. Moreover, considering the rapid reactivity of sulphur and phosphorus with a fresh iron surface [34,35] and the rubbing between crack faces induced by displacement during crack growth [36], it is reasonable to conclude that ZDDP tribofilm was produced on the crack faces. Fig. 14 (e) shows the EDS profile on a crack path in Test 8 (λ = 0.24, SRR=−20 %, 6 million cycles), which also confirmed the formation of ZDDP tribofilm on crack faces.

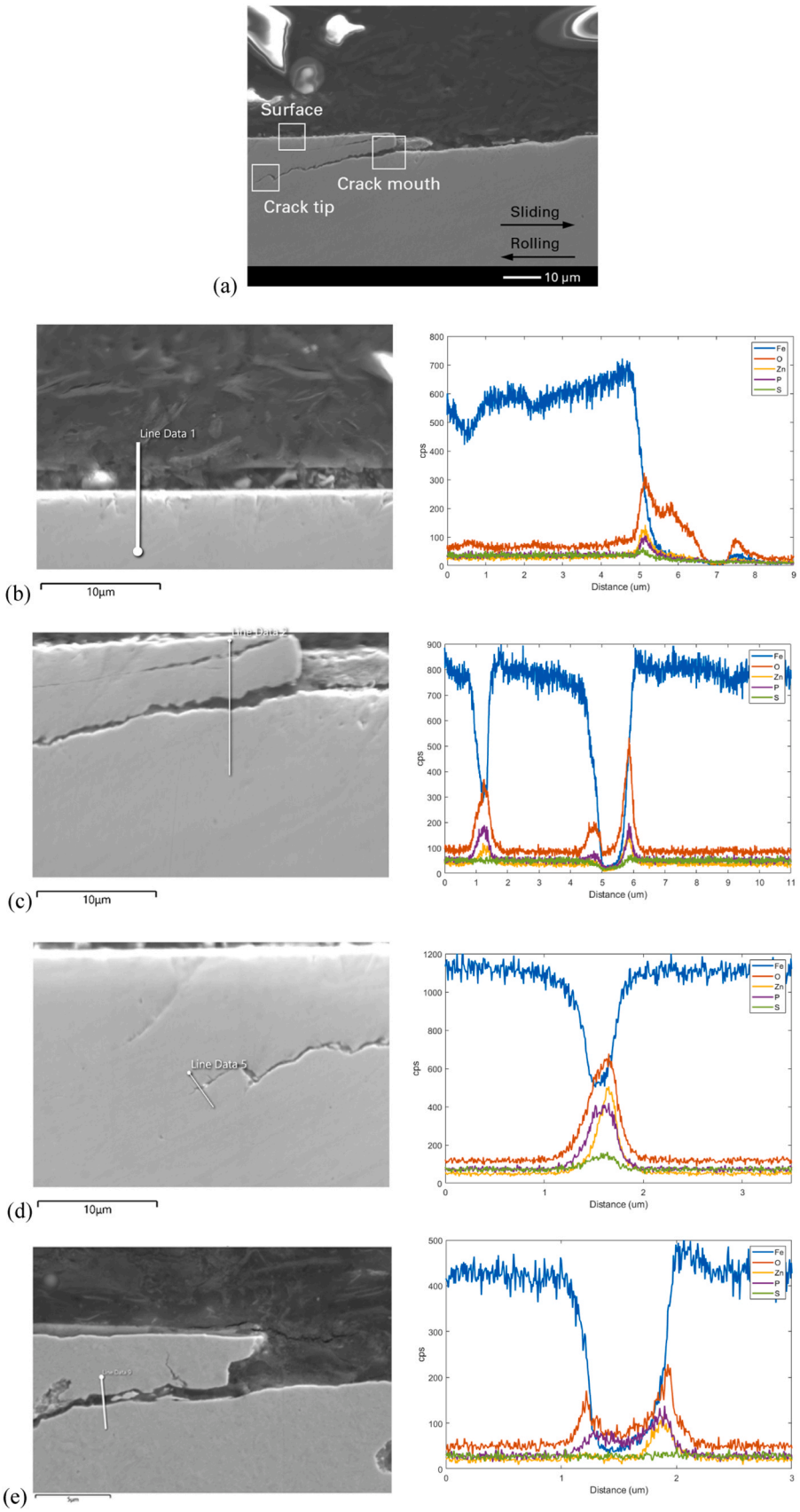

Fig. 14. (a) Positions for EDS analysis in Test 4 (λ = 0.23, SRR=−10 %, 6 million cycles), (b) EDS line on the disc surface and corresponding EDS profile in Test 4, (c) EDS line on the crack mouth and corresponding EDS profile in Test 4, (d) EDS line on the crack tip and corresponding EDS profile in Test 4, (e) EDS line on the crack tip and corresponding EDS profile in Test 8 (λ = 0.24, SRR=−20 %, 6 million cycles).

As shown in Fig. 4, by 6 million cycles, the number of cracks increased in the base oil only tests with lambda ratios of 0.23–0.24 (Tests 3 and 7) and they grew into large-scale macropitting, while in the base oil + ZDDP test (Tests 4 and 8), only the number of micropits increased slightly without seeing an increase in the dimensions. Considering the analysis in Fig. 14, the slow progression of micropitting in the base oil + ZDDP tests can be attributed to the high crack face friction caused by the ZDDP tribofilm produced on crack faces as depicted in Fig. 15. Once a crack initiates, the crack face friction becomes a dominant factor in crack propagation. When the crack faces come into contact, their rubbing is influenced by the crack face friction f_c. An increase in f_c leads to reduced slip between crack faces which is indicated by a decrease in ΔK_{II} [23,24] as indicated by the modelling work presented in [23]. The reduced slip slows down the crack growth [23,24], consequently retarding the progression of micropitting into macropitting.

4. Conclusions

This study has investigated the effect of ZDDP additive in the formation and progression of micropitting by conducting experiments on a TE74 twin-disc tribometer. Lubricant chemistry, friction, and wear are shown to be important factors for micropitting behaviour. Lambda ratio and sliding are also found to influences wear, friction, and extent of microitting. The following conclusions were drawn based on the experimental results.

1. A twin-disc tribometer offers a suitable platform for generating and investigating both micropitting (with depth up to 20 μm) and macropitting (with depth of tens of microns). For both base oil and ZDDP-enriched oil, pitting were produced under boundary and mixed lubrication conditions.
2. In base oil tests, more wear and lower friction were identified. Cracks initiated later, but progressed rapidly into macropits. Conversely, when using ZDDP-enriched oil, the friction was higher and micropits initiated rapidly, however, their progression was slow.
3. The mechanism through which the ZDDP additive influences micropitting formation involves its capacity to mitigate wear and increase friction on contacting surfaces. ZDDP tribofilm formed on the contacting surfaces maintains asperities and the number of asperity stress cycles remains high. Moreover, ZDDP tribofilm contributes to increased surface friction, which heightens the tensile and shear stresses in the regions close to the surface, leading to increased fatigue damage accumulation and micropitting damage.
4. The mechanism by which the ZDDP additive affects micropitting progression involves the increased friction on crack faces induced by ZDDP tribofilm. This internal ZDDP tribofilm increases the friction between crack faces, leading to decreased crack face slip, slowing down the crack propagation and consequently limiting the progression of micropitting. The findings serve to address debates regarding the effect of ZDDP on micropitting and contribute to a deeper understanding of the underlying mechanisms.
5. In practical bearing applications, bearing surfaces do not frequently suffer from micropitting. This work used relatively rough surfaces and severe contact conditions to accelerate pitting formation. Considering the findings obtained from this work, anti-wear additives such as ZDDP protect surfaces from wear and impede the progression of micropitting, which is beneficial for bearing operations.

Statement of originality

I, Zaihao Tian, hereby declare that the manuscript titled “Influence of ZDDP Tribofilm on Micropitting Formation and Progression” submitted to Tribology International, published by Elsevier, is entirely my own original work. I affirm that:

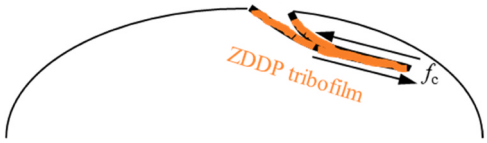

Fig. 15. Effect of ZDDP tribofilm on crack face friction and crack propagation.

2. The content of this manuscript is the result of my independent research efforts, and I have not used any unauthorized or uncredited sources in the development of this paper.
3. All ideas, data, and concepts presented in this manuscript are my own, except where I have explicitly cited and referenced the work of others in accordance with established academic conventions.
4. I have not submitted this manuscript for publication elsewhere, and it is not under consideration for publication in any other journal or conference proceeding.
5. The figures, tables, and other graphical representations included in this manuscript are original, or appropriate permissions and attributions have been obtained for their use.
6. This manuscript has not been previously published, in whole or in part, in any form, including online publications or preprints, nor is it currently being considered for publication in any other publication outlet.
7. Any potential conflicts of interest related to the research or the publication of this manuscript have been disclosed in accordance with the guidelines provided by [Journal Name] and Elsevier.

I acknowledge that the submission of a manuscript containing false or misleading information is a serious violation of academic ethics and publication standards. I understand that if any of the statements in this declaration are found to be untrue, it may result in the rejection of my submission or, if the paper has already been published, its retraction.

I am willing to provide further clarification or documentation regarding the originality and authenticity of this manuscript if required by the editorial board of [Journal Name].

CRediT authorship contribution statement

Shuncai Wang: Supervision, Investigation. **Ping Lu:** Writing – review & editing, Writing – original draft, Methodology, Investigation. **Zaihao Tian:** Writing – review & editing, Writing – original draft, Visualization, Investigation. **Robert Wood:** Writing – review & editing, Supervision, Methodology, Funding acquisition, Conceptualization. **Daniel Merk:** Supervision, Resources.

Declaration of Competing Interest

The authors declare the following financial interests/personal relationships which may be considered as potential competing interests: Zaihao Tian reports financial support was provided by Schaeffler Technologies AG & Co KG.

Data Availability

No data was used for the research described in the article.

Acknowledgements

The authors would like to thank the Engineering and Physical Sciences Research Council (EPSRC) funding: EP/S005463/1 Early detection of contact distress for enhanced performance monitoring and predictive inspection of machines for providing financial support for this work.

The authors would like to thank Schaeffler Technologies AG & Co.

KG, Herzogenaurach, Germany for providing financial support and test samples for this work.

References

[1] Rycerz P, Olver A, Kadiric A. Propagation of surface initiated rolling contact fatigue cracks in bearing steel. Int J Fatigue 2017;97:29–38.
[2] Sadeghi, F., et al., *A review of rolling contact fatigue*. 2009.
[3] Santus C, et al. Surface and subsurface rolling contact fatigue characteristic depths and proposal of stress indexes. Int J Fatigue 2012;45:71–81.
[4] Errichello R. Morphology of micropitting. Gear Technol 2012;4:74–81.
[5] Kissling U. Application of the first international calculation method for micropitting. Gear Technol 2012;5:54–60.
[6] Rycerz P, Kadiric A. The influence of slide–roll ratio on the extent of micropitting damage in rolling–sliding contacts pertinent to gear applications. Tribology Lett 2019;67:1–20.
[7] Morales-Espejel GE, Brizmer V. Micropitting modelling in rolling–sliding contacts: application to rolling bearings. Tribology Trans 2011;54(4):625–43.
[8] Symonds N. *Rolling contact fatigue–review and case study.*. in *Conference Proceedings NATO-RTA-AVT-109: The Control and Reduction of Wear in Military Platforms*. Session,; 2004.
[9] Corni I, et al. Characterization and mapping of rolling contact fatigue in rail-axle bearings. Eng Fail Anal 2017;82:617–30.
[10] Ueda M, Spikes H, Kadiric A. In-situ observations of the effect of the ZDDP tribofilm growth on micropitting. Tribology Int 2019;138:342–52.
[11] Dawczyk J, et al. Film thickness and friction of ZDDP tribofilms. Tribology Lett 2019;67:1–15.
[12] Spikes H. The history and mechanisms of ZDDP. Tribology Lett 2004;17(3):469–89.
[13] Soltanahmadi S, et al. Experimental observation of zinc dialkyl dithiophosphate (ZDDP)-induced iron sulphide formation. Appl Surf Sci 2017;414:41–51.
[14] Fujita H, Spikes H. The formation of zinc dithiophosphate antiwear films. Proc Inst Mech Eng, Part J: J Eng Tribology 2004;218(4):265–78.
[15] Lainé E, Olver A, Beveridge T. Effect of lubricants on micropitting and wear. Tribology Int 2008;41(11):1049–55.
[16] Benyajati C, Olver A, Hamer C. An experimental study of micropitting, using a new miniature test-rig. in *Tribology Series*. Elsevier,; 2003. p. 601–10.
[17] Zhang J, et al. Boundary friction of ZDDP tribofilms. Tribology Lett 2021;69(1):17.
[18] Ueda M, et al. The effect of friction on micropitting. Wear 2022;488:204130.
[19] Sato K, Watanabe S, Sasaki S. High friction mechanism of ZDDP tribofilm based on in situ AFM observation of nano-friction and adhesion properties. Tribology Lett 2022;70(3):94.
[20] Brizmer V, et al. The influence of tribolayer formation on tribological performance of rolling/sliding contacts. Tribology Lett 2017;65(2):57.
[21] Vrček A, et al. Micro-pitting damage of bearing steel surfaces under mixed lubrication conditions: effects of roughness, hardness and ZDDP additive. Tribology Int 2019;138:239–49.
[22] Airey J, et al. The effect of aviation anti-wear additives on tribofilm formation and micropitting propensity. Proc Inst Mech Eng, Part J: J Eng Tribology 2023. 13506501231167621.
[23] Benuzzi D, Bormetti E, Donzella G. Stress intensity factor range and propagation mode of surface cracks under rolling–sliding contact. Theor Appl Fract Mech 2003;40(1):55–74.
[24] Baietto M-C, Pierres E, Gravouil A. A multi-model X-FEM strategy dedicated to frictional crack growth under cyclic fretting fatigue loadings. Int J Solids Struct 2010;47(10):1405–23.
[25] Zhou Y, et al. The effect of contact severity on micropitting: Simulation and experiments. Tribology Int 2019;138:463–72.
[26] Stratmann A, et al. Antiwear tribofilm growth in rolling bearings under boundary lubrication conditions. Tribology Int 2017;113:43–9.
[27] Tian Z, et al. Condition monitoring of pitting evolution using multiple sensing. in *Proceedings of the International Conference on Condition Monitoring and Asset Management*. The British Institute of Non-Destructive Testing,; 2023.
[28] Kim T, Olver A. Stress history in rolling–sliding contact of rough surfaces. Tribology Int 1998;31(12):727–36.
[29] Leiro A, et al. Wear of nano-structured carbide-free bainitic steels under dry rolling–sliding conditions. Wear 2013;298:42–7.
[30] Ryttberg K, et al. The effect of cold ring rolling on the evolution of microstructure and texture in 100Cr6 steel. Mater Sci Eng: A 2010;527(9):2431–6.
[31] Zhang J, Spikes H. On the mechanism of ZDDP antiwear film formation. Tribology Lett 2016;63:1–15.
[32] Brizmer V, Pasaribu H, Morales-Espejel GE. Micropitting performance of oil additives in lubricated rolling contacts. Tribology Trans 2013;56(5):739–48.
[33] Morales-Espejel G, Rycerz P, Kadiric A. Prediction of micropitting damage in gear teeth contacts considering the concurrent effects of surface fatigue and mild wear. Wear 2018;398:99–115.
[34] Meheux M, et al. Effect of lubricant additives in rolling contact fatigue. Proc Inst Mech Eng, Part J: J Eng Tribology 2010;224(9):947–55.
[35] Minfray C, et al. Experimental simulation of chemical reactions between ZDDP tribofilms and steel surfaces during friction processes. Tribology Lett 2006;21:65–76.
[36] Kunzelmann B, et al. Prediction of rolling contact fatigue crack propagation in bearing steels using experimental crack growth data and linear elastic fracture mechanics. Int J Fatigue 2023;168:107449.